

Comparison of an efficient implementation of gray molasses to narrow-line cooling for the all-optical production of a lithium quantum gas

C. L. Satter,¹ S. Tan,¹ and K. Dieckmann^{1,2,*}

¹*Centre for Quantum Technologies (CQT), 3 Science Drive 2, Singapore 117543*

²*Department of Physics, National University of Singapore, 2 Science Drive 3, Singapore 117542*

(Dated: August 22, 2018)

We present an efficient scheme to implement a gray optical molasses for sub-Doppler cooling of ${}^6\text{Li}$ atoms with minimum experimental overhead. To integrate the D_1 light for the gray molasses (GM) cooling into the same optical set-up that is used for the D_2 light for a standard magneto-optical trap (MOT), we rapidly switch the injection seeding of a slave laser between the D_2 and D_1 light sources. Switching times as short as $30\ \mu\text{s}$ can be achieved, inferred from monitor optical beat signals. The resulting low-intensity molasses cools a sample of $N = 9 \times 10^8$ atoms to about $60\ \mu\text{K}$. A maximum phase-space density of $\rho = 1.2 \times 10^{-5}$ is observed. On the same set-up, the performance of the GM is compared to that of narrow-line cooling in a UV MOT, following the procedure in [1]. Further, we compare the production of a degenerate Fermi gas using both methods. Loading an optical dipole trap from the gray molasses yields a quantum degenerate sample with 3.3×10^5 atoms, while loading from the denser UV MOT yields 2.4×10^6 atoms. Where the highest atom numbers are not a priority this implementation of the gray molasses technique yields sufficiently large samples at a comparatively low technical effort.

PACS numbers: 37.10.De, 37.10.Gh, 67.85.Lm, 42.60.Fc

I. INTRODUCTION

Ultracold quantum gases of neutral atoms have emerged as an ideal testing ground for quantum many-body physics [2, 3]. Lithium is particularly suitable for this purpose due to the presence of a broad, magnetically tunable Feshbach resonance, which allows its two-body interactions to be varied over a wide range. For the production of a quantum degenerate sample, a sufficiently high phase-space density is necessary to initiate efficient evaporative cooling. For most species in the alkali-metal group this can be achieved by standard Doppler and sub-Doppler laser cooling on the D_2 transition. However for lithium (and potassium), standard laser cooling to sub-Doppler temperatures using the D_2 transition is inefficient. This is due to the fact that this transition is characterized by an unresolved hyperfine structure of the $2P_{3/2}$ excited state [4]. Cooling schemes for lithium that circumvent this problem are therefore of great interest, and efforts to improve these schemes form an active area of research.

So far, two robust methods are available that achieve cooling below the Doppler limit for ${}^6\text{Li}$. In narrow-line cooling of alkali atoms [1, 5, 6], a magneto-optical trap (MOT) is realized on the transition to the higher excited $3P_{3/2}$ state. This transition has a narrower linewidth and correspondingly a lower Doppler temperature. This technique was successfully used in our set-up to create cold, dense samples of ${}^6\text{Li}$ atoms [1], and to produce weakly-interacting quantum-degenerate Fermi gases and molecular BECs [7].

The other cooling method is the gray optical molasses, which has been successfully employed in a series of experiments involving various alkali atoms [8–19]. This method combines velocity-selective coherent population trapping (VSCPT) into dark states with a friction force arising from a Sisyphus mechanism [20–22]. The gray molasses operates on the open atomic transitions $F \rightarrow F$ and $F \rightarrow F - 1$, for which Λ -shaped energy level structures are available that allow the occurrence of dark states. Therefore, the gray molasses is commonly applied on the D_1 transition. In many previous experiments a separate laser system was used to generate the light at the D_1 transition. Often, the D_1 and D_2 frequency beams are superimposed as a final step before being guided to the experiment using an optical fiber. In this way, D_1 gray molasses can be performed subsequently to standard D_2 loading of a MOT.

For the all-optical production of quantum degenerate gases it can be beneficial to enhance the number density of the atomic sample for improved loading into an optical dipole trap (ODT). The gray molasses method does not provide a confinement force during the cooling, and hence does not actively increase the density. In this case, an improved ODT loading efficiency can only be realized with additional experimental effort, e.g. by increasing the spatial overlap between the cooled cloud and the ODT (see e.g. [14]), or by adapting the pre-cooling stages to achieve higher initial densities before applying the GM (see e.g. [13]).

In this article we present an efficient implementation of simple gray molasses (GM) cooling on the D_1 transition for ${}^6\text{Li}$ that minimizes experimental overhead. This implementation leads to the production of a degenerate Fermi gas without additional methods to enhance the ODT loading. For our implementation of the gray

* Electronic address: phydk@nus.edu.sg

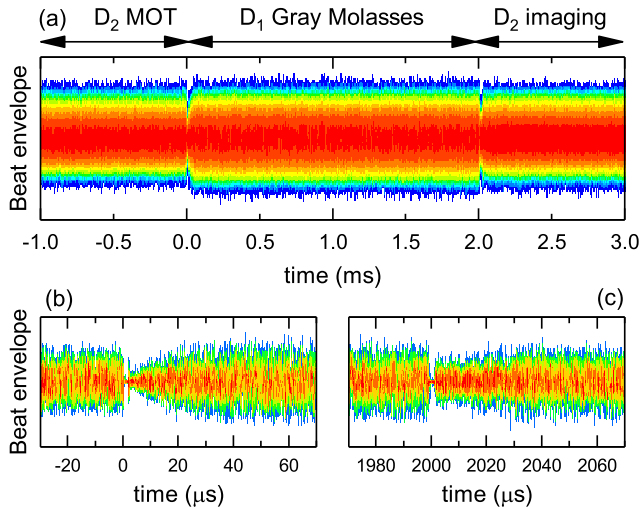


FIG. 2. The envelope of the D_2 and D_1 beats as a function of time during the experimental sequence. Here, the sample density is displayed, as the beat signals are rapidly oscillating (> 100 MHz) on the observed timescales. Warmer colors represent higher sample density. At $t = 0$, the D_2 light was switched off, and the path was opened for the D_1 light to seed the DL. After 2.0 ms of gray molasses cooling, the source for seeding the DL is switched back to the D_2 ECDL for absorption imaging. Panel (a) shows the beat PD signal over the entire beat sequence, while panels (b) and (c) show the signal at the switch-over points with higher time resolution.

gray molasses cooling [10]. For the purpose of controlling the parameters relevant for GM cooling, AOM1 is used to obtain the required detuning δ_{cool} to the blue side of the D_1 cooling transition. The two AOMs before the fiber cluster control the intensities of the cooling and repumping light, respectively I_{cool} and I_{rep} , and the detuning δ_{rep} of the repumping light.

Since the frequencies of the D_1 and D_2 atomic transitions are separated by only 10.1 GHz, the slave diode laser can be injection seeded by either source ECDL. However, the different light frequencies match the laser diode cavity modes at different values of the DL operating current. To quickly switch between the two, as is done when progressing from the MOT cooling stage to the gray molasses, a current modulation pulse is sent to the DL. Because gray molasses cooling is only applied for a few milliseconds, a single modulation current value is typically sufficient. Temperature fluctuations due to the sudden change in injection current are negligible for timescales up to at least 10 ms, as was observed by varying the duration of the gray molasses phase.

As a convenient method to monitor whether the DL is truly following the D_1 frequency for the entire duration of gray molasses cooling and how quickly it does so, a beat system was set up. The zero-order beams from AOM1 after the D_1 ECDL and AOM3 after the DL are overlapped onto a photodiode (PD), as is indicated by the dashed beam paths in Fig. 1(b). When the DL follows

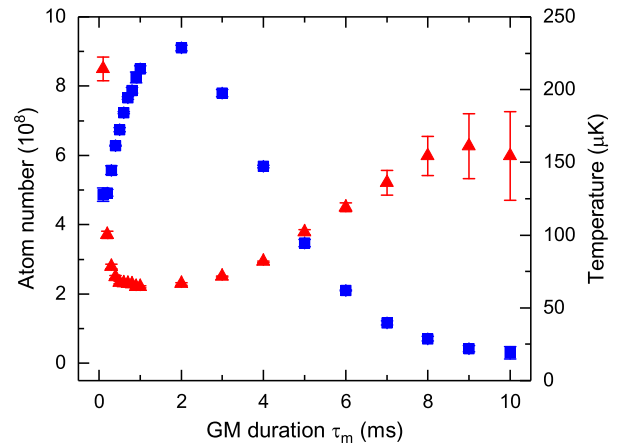


FIG. 3. Temporal evolution of the gray molasses. The number of captured atoms N (blue squares) and temperature T (red triangles) are plotted as a function of the molasses duration τ_m . The data correspond to the gray molasses at a magnetic bias field of -0.9 G.

the optical frequency dictated by the D_1 ECDL, a beat appears at a frequency of 156 MHz, which is twice the frequency applied to AOM1. In the experiment we monitor the beat by observing its envelope. If no injection locking is established the beat ceases and the observed amplitude vanishes. Using this method, the response of the slave DL can be monitored during the experiment and, if necessary, be acted upon accordingly, e.g. by adjusting the modulation current to the DL. An example of a typical signal as observed during the experimental sequence is shown in Fig. 2(a). When the trapping and cooling cycle is completed, the atomic ensemble is imaged using laser light at the D_2 frequency. For this purpose, the source for seeding the slave laser needs to be switched back to the D_2 ECDL. To monitor that this happens correctly and quickly enough, another beat is produced, this time between the D_2 ECDL and DL outputs. In practice we see, as shown in Fig. 2(b) and (c), that the DL can switch very quickly between the two light sources, with a gap of only $\approx 30 \mu\text{s}$ in between during which it is not properly seeded.

III. THE GRAY MOLASSES

Before GM cooling is applied, our experimental sequence starts with a standard 3D MOT on the D_2 transition. After 15 s of loading from a Zeeman-slowed atomic beam, the MOT is compressed by simultaneously decreasing the detuning and light intensity, and increasing the gradient of the magnetic quadrupole field. At the end of the compression phase 1.9×10^9 atoms remain in the compressed MOT (cMOT), at a peak density of $n_0 = 3.5 \times 10^{10} \text{ cm}^{-3}$. From time-of-flight absorption images we infer a typical temperature of $800 \mu\text{K}$.

In preparation for the gray molasses cooling stage, the

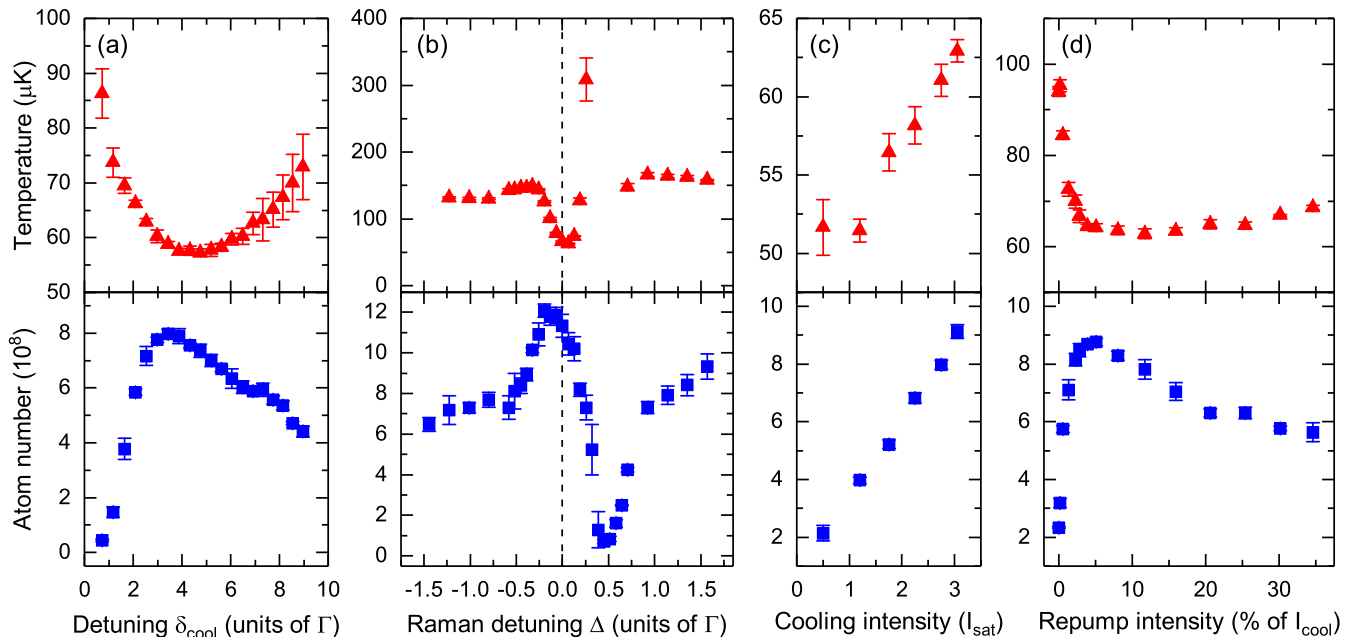


FIG. 4. Number of cooled atoms (blue squares) and temperature (red triangles) as a function of (a) the detuning δ_{cool} , (b) the Raman detuning Δ between repumping and cooling light, (c) the intensity of the cooling light, and (d) the intensity of the repumping light. For (b), around $\Delta = 0.5\Gamma$ the temperature data are not presented, as a partially heated cloud was observed.

D_2 light is extinguished and the magnetic quadrupole field is switched off. In our chamber this induces a magnetic eddy field to which the gray molasses cooling proved sensitive. In order to allow the field to decay, the D_1 light is turned on by the AOMs in front of the fiber cluster only after a delay of 0.5 ms. The earth field as well as the remaining eddy field were compensated by applying a constant bias field during GM cooling. In the direction along the axis of the MOT coils, which required the most significant compensation, a bias field of -0.9 G was applied. This value was chosen to yield the lowest temperatures at short molasses durations. We measured a quadratic increase in temperature of $\Delta T \propto 210\ \mu\text{K}/\text{G}^2$ when deviating from this optimum.

A. Characterization

We first studied the evolution of the gray molasses over time. In Fig. 3 the atom number N and temperature T are plotted against the duration τ_m of the D_1 molasses pulse. For these measurements an overall blue detuning of $\delta_{\text{cool}} = 3.2\Gamma$ and an intensity of $I_{\text{cool}} = 3.1 I_{\text{sat}}$ were used. Here, $\Gamma = 2\pi \times 5.87\text{ MHz}$ is the natural linewidth and I_{sat} refers to the saturation intensity of the D_2 transition. The Raman detuning between cooling and repumping light was kept constant at $\Delta = \delta_{\text{rep}} - \delta_{\text{cool}} = -0.045\Gamma$ and I_{rep} was kept at 5% of I_{cool} . The sample temperature was observed to decrease rapidly during the first 0.5 ms, and reached a minimum of $T \simeq 64\ \mu\text{K}$. At $\tau_m = 2\text{ ms}$, a

maximum of 50% of cMOT atoms was captured by the molasses and cooled. After $\tau_m = 3\text{ ms}$ however, the temperature started to rise and the atom number dropped. This is attributed to the fact that the magnetic bias field applied compensates well for the eddy fields that are present during the first few milliseconds of the cooling stage, but is not optimal for longer durations, when the eddy fields have further decayed.

In the following, we describe the effect of different parameters on the performance of the gray molasses for a 2 ms GM pulse duration, as summarized in Fig. 4. Varying the overall laser detuning the capture efficiency and cloud temperature reach optima at a blue detuning of $\delta_{\text{cool}} = 4\Gamma$ with respect to the D_1 transition, as can be seen from Fig. 4(a). Upon increasing the detuning further, the captured atom number decreases, and cooling is less effective. This is expected, since for optical molasses the capture velocity is proportional to $1/\delta^2$.

To show the sensitivity of the GM cooling to the Raman detuning Δ we pre-cooled the cloud at $\Delta = -0.045\Gamma$ for 2 ms and applied a 0.25 ms pulse at a variable Raman detuning. As can be seen from Fig. 4(b), cooling is optimal at exact Raman resonance, while the number of atoms captured displays a clear maximum for a small, red Raman detuning $\Delta = -0.2\Gamma$. For Δ chosen slightly blue of the Raman condition, a strong heating of the cloud occurs, accompanied by a sharp decrease in the number of cooled atoms. The observed Fano profile formed by the dependence of atom number and temperature on Δ has become a signature of gray molasses

cooling (see e.g. [11–13]). The strong contribution of the repumper and the enhanced cooling near the Raman condition point to the existence of long-lived coherences between the two hyperfine manifolds $|2S_{1/2}, F = 3/2\rangle$ and $|2S_{1/2}, F = 1/2\rangle$. In the presence of the repumper, a second Λ -type three-level system is formed, with new inter-manifold dark states and bright states [11].

The effect of the intensity of the GM cooling light on the atoms is shown in Fig. 4(c). During this measurement, the ratio $I_{\text{rep}}/I_{\text{cool}}$ was kept constant. We observe that, as the cooling intensity is increased, the number of atoms captured by the molasses increases linearly. This is in agreement with the dependence of the capture velocity on the intensity, as $v_{\text{cap}} \sim \Gamma_{\text{p}}/k$, where $\Gamma_{\text{p}} \propto I/\delta^2$ is the optical pumping rate. Since the trend is not yet seen to saturate at $I_{\text{cool}} = 3I_{\text{sat}}$, we expect that a larger number of atoms can be captured into the molasses by using higher-intensity D_1 beams. The temperature of the molasses is observed to increase linearly with the intensity. This is expected, as the equilibrium temperature pertaining to a Sisyphus cycle scales with the light shift as $T \propto I/\delta$ [10].

The intensity of the repumper I_{rep} with respect to the cooling intensity I_{cool} also turned out to play an important role. In Fig. 4(d), the captured atom fraction and temperature are plotted against I_{rep} in units of percentage of I_{cool} . The captured atom fraction shows a clear maximum at 5.5%, which corresponds to a repumping intensity of $I_{\text{rep}} = 0.12I_{\text{sat}}$. The decrease in atom number for increased repumping power can be attributed to increased photon reabsorption of the scattered light on the cooling transition, as the optical density of the cloud with respect to the cooling transition increases with the repumper intensity [23].

In our experiment, the coldest temperature after the gray molasses was observed when the Raman detuning was tuned to exact $\Delta = 0$, for the full GM duration of 2 ms. Then, a temperature of $41(2) \mu\text{K}$ can be obtained, at the cost of the captured atom number being reduced to half of the maximum value. Presumably, even lower temperatures can be reached by using a low cooling light intensity. Several gray molasses experiments (e.g. [10, 13, 15, 16]) take advantage of the relationship between cooling intensity and temperature to implement a two-stage GM. A high intensity is used to maximize the capture efficiency, after which the intensity is ramped down to obtain lower temperatures. In our set-up, this method was observed not to yield a temperature improvement. In this we believe we are limited by the low available beam intensity and long-lived eddy fields, which prevent us from using the GM for a duration long enough to implement intensity ramps.

We calculate the phase-space density from $\rho = n_0\Lambda_T^3$, where $\Lambda_T = \frac{h}{\sqrt{2\pi mk_{\text{B}}T}}$ is the thermal de Broglie wavelength and k_{B} is the Boltzmann constant. The highest phase-space density is attained at $\Delta = -0.05\Gamma$ and 2 ms GM duration. Up to $N = 9 \times 10^8$ cooled atoms are detected in the gray molasses, at a temperature of around

$60 \mu\text{K}$. This corresponds to a captured fraction of 50% from the cMOT. The peak density was inferred from *in situ* imaging. As noted earlier, there are no confinement or compression forces present during the gray molasses, and hence the peak density does not increase during GM cooling. Since a fraction of the atoms remains uncooled by the molasses, the peak density decreases with respect to the cMOT to $n_0 = 2 \times 10^{10} \text{ cm}^{-3}$. This results in a maximum phase-space density of $\rho = 1.2 \times 10^{-5}$.

B. Comparison with narrow-line MOT

In the following we compare the results from the GM cooling to the narrow-line MOT previously described in [1], which employs the $2S_{1/2} \rightarrow 3P_{3/2}$ at an ultraviolet (UV) wavelength. For this purpose the UV MOT is loaded after an initial MOT stage on the D_2 transition, which is almost identical to the one used in the GM experiment. However, due to the different magnetic field requirements of the UV MOT, the bias fields during both the red MOT and UV MOT stage are allowed to take on more beneficial values as compared to the situation where the GM scheme is used. This leads to a lower red cMOT temperature of $T = 480 \mu\text{K}$ with a total number of atoms of $N = 1.4 \times 10^9$ captured.

The parameters for the UV MOT are similar to the ones previously described. For repumping light the red D_2 transition is used. The UV MOT is loaded for 1.5 ms at a detuning of $-8\Gamma_{3\text{P}}$ and magnetic field gradient of 3.4 G/cm to optimize the number of atoms captured from the red cMOT. In another 1.5 ms a compression is carried out, during which the detuning is ramped up to $-2.9\Gamma_{3\text{P}}$ and the field gradient is increased to 12 G/cm . After compression is completed, the UV MOT reaches a transient maximum in phase-space density after another 16 ms of hold time.

In the current measurements, 1.3×10^8 atoms were observed to be present in the UV MOT after the compression stage, at a temperature of $T = 70 \mu\text{K}$. This leads to a peak density of $n_0 = 1.2 \times 10^{11} \text{ cm}^{-3}$ and phase-space density of $\rho = 7 \times 10^{-5}$ after the UV cMOT.

When it comes to the peak density of the atomic cloud, narrow-line cooling in the UV MOT has the distinct advantage that it operates in the presence of a magnetic quadrupole field. This means that the atoms can be spatially confined during cooling, and can be compressed by increasing the magnetic field gradient. Moreover, in our set-up the UV MOT cooling beams are independent of the beams for the D_2 MOT, providing us with the flexibility to choose a smaller $1/e^2$ beam waist of 4.3 mm . The result is that peak density and phase-space density are approximately a factor of six higher as compared to the values attained for the case of gray molasses cooling. In the following we investigate how this difference affects the transfer efficiency into the small volume and limited depth of an optical dipole trap and evaporative cooling into quantum degeneracy.

IV. PRODUCTION OF A STRONGLY INTERACTING FERMI GAS

In this section we investigate the suitability of our implementation of the gray molasses for the all-optical production of a lithium quantum gas. We directly compare this to the results obtained with narrow-line cooling. For this purpose we follow the same procedure as previously described in detail in [7]. In this scheme the pre-cooled atoms are transferred into a two-beam, small-angle, crossed optical dipole trap (ODT), transported from the MOT vacuum chamber into a glass science cell, and are evaporatively cooled. For the purpose of evaporative cooling of the fermions we make use of the broad Feshbach resonance in the spin mixture of the two energetically lowest Zeeman levels $|F = 1/2, m_F = \pm 1/2\rangle$ (commonly referred to as states $|1\rangle$ and $|2\rangle$). Our crossed optical dipole trap has a transverse beam waist of $66 \mu\text{m}$. For the measurements presented here we start evaporation with an initial optical power of 22.5 W per beam. This corresponds to a trap depth of approximately of $k_B \times 330 \mu\text{K}$ and axial and radial trap frequencies of $\omega_z = 2\pi \times 64(9) \text{ Hz}$ and $\bar{\omega}_r = \sqrt{\omega_x \omega_y} = 2\pi \times 2.81(3) \text{ kHz}$, respectively.

A. Loading the ODT from the gray molasses

For the transfer of the atoms into the ODT from the gray molasses, the optical power is ramped up within 0.5 ms to the full trap depth at the start of the GM phase. Both the GM and ODT beams are on for 1.5 ms , during which time the gray molasses reaches its highest density, and coldest conditions. We observed heating and atom loss from the trap for longer cooling periods as expected from the measurements of the gray molasses presented in Fig. 3. The GM is then switched off by extinguishing the repumping light in advance of the cooling light, to optically pump the atoms into the $|F = 1/2\rangle$ hyperfine ground state manifold. This creates an incoherent balanced mixture of the $|1\rangle$ and $|2\rangle$ states.

While the operating wavelength of 1070 nm for the ODT was chosen to be near the magic wavelength [24] for the UV MOT transition, this is not the case for the gray molasses. Hence, it is worth investigating the possibility that the light shift induced by the ODT could affect the efficacy of GM cooling by shifting the global detuning of the cooling light. We investigated the effect by varying the detuning of the gray molasses light during the combined cooling and optical trapping stage. Fig. 5 shows the atom number yield. As can be seen from Fig. 5(a), no significant shift was observed, if δ_{cool} was varied. This is consistent with the experimental determination by Burchianti *et al.* [14] of a light-shift coefficient of $+6.3(7) \text{ MHz}/(\text{MW}/\text{cm}^2)$ for the case of a $\lambda = 1073 \text{ nm}$ trapping laser wavelength. From this we expect for our ODT power a frequency shift of 2 MHz , less than a natural linewidth. The critical sensitivity of the atom number

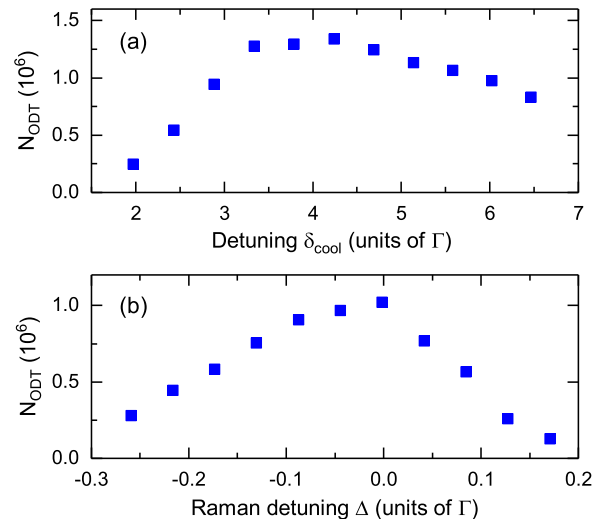


FIG. 5. (Color online) The number of atoms captured from the GM into the ODT as a function of (a) the overall detuning δ_{cool} , and (b) the Raman detuning Δ .

yield to the Raman detuning Δ was observed in the ODT as well, as shown in Fig. 5(b). This demonstrates the dependence of the loading efficiency on the phase-space density produced by the GM.

Immediately after loading, we observe that $N = 1.35 \times 10^6$ atoms are transferred to the optical dipole trap. The temperature is $T = 63 \mu\text{K}$. Following the loading, we allow for 1 s of plain evaporation. For the purpose of thermalization, a magnetic bias field of approximately 200 G is applied. This tunes the s-wave scattering length between the two states to $a_{12} = -220 a_0$ [25], where a_0 is the Bohr radius. After plain evaporation the ODT typically contains a total number of atoms of $N = 1.1 \times 10^6$ at a temperature of $T = 43 \mu\text{K}$, corresponding to $T/T_F = 7.3$, where T_F is the Fermi temperature. This corresponds to an initial truncation parameter of $\eta = 7.7$ before forced evaporation is applied.

B. Loading the ODT from the UV MOT

We perform a similar loading sequence when the ODT is loaded from the UV MOT. For the transfer of the atoms into the crossed ODT, the optical power is linearly ramped up within 3 ms to the full trap depth during the compressed UV MOT phase. A combined loading and cooling duration of 11 ms is used, in order to allow for the peak density to reach its transient maximum value. Afterwards, the UV MOT is switched off and hyperfine pumping and plain evaporation are done in the same manner as described in the previous section for the GM case. Afterwards, the ODT typically contains a total number of atoms of $N = 7.5 \times 10^6$ at a temperature of $45 \mu\text{K}$ corresponding to $T/T_F = 4.2$ and

a truncation parameter of $\eta = 7.3$ before initiating forced evaporation. The atom number found is about a factor of seven higher as compared to the GM case, which is in good agreement with the ratio in phase space density produced by the two cooling methods.

C. Evaporation to degeneracy

To facilitate creating a strongly interacting quantum gas in the BEC-BCS crossover regime, forced evaporation is performed near the broad 832 G Feshbach resonance. Here, we apply a magnetic bias field of 940 G to evaporate on the BCS side above the resonance. At this field the s -wave scattering length is $a_{12} = -5100 a_0$ [25], establishing rapid thermalization during the cooling. The trap depth is reduced according to the theoretical curve $U_0(t) = U_0(0)(1 - t/\tau_u)^{2(\eta'-3)/(\eta'-6)}$, which was derived by Luo *et al.* [26] for a Fermi gas mixture with a unitarity-limited s -wave scattering cross section. η' is related to the truncation parameter by $\eta' = \eta + (\eta - 5) / (\eta - 4)$.

For the GM case we use a time constant of $\tau_u = 10$ s, which was experimentally optimized for maximum atom number. For this time constant it takes about 8.5 s to lower the optical power to about 40 mW per beam, at which point atoms are increasingly spilled from the trap. To characterize the evaporation we probe the atomic cloud at various intermediate optical powers during the evaporation ramp. The images are fitted to a Fermi profile, from which we extract atom number, temperature, and T/T_F . The results are shown in Fig. 6(a). We observe efficient cooling of the cloud down to a laser power of $P = 93$ mW/beam, where $3.3(3) \times 10^5$ atoms remain trapped at a temperature of 96(7) nK, corresponding to $T/T_F = 0.30(2)$. The atom number rapidly decreases with lower optical powers, which indicates that atoms are spilling from the trap, as the trap depth is lowered below the Fermi energy.

For the case of loading from the UV MOT the time constant for evaporation ramp is allowed to be smaller, due to a higher initial density of atoms in the ODT. Here, a time constant of $\tau_u = 3$ s was used corresponding to a duration of 2.6 s. The results are presented in Fig. 6(b). The temperature as a function of trap depth follows a nearly identical curve as in Fig. 6(a), especially at higher trap depths. Evaporation is seen to be efficient down to optical powers of 93 mW, where $2.4(1) \times 10^6$ atoms remain trapped at a temperature of 175(8) nK, corresponding to $T/T_F = 0.28(1)$. As expected the atom number in the quantum degenerate regime is higher than for the GM case. The relative factor of about seven found at the end of the plain evaporation stage remains nearly constant throughout the forced evaporation ramp. The higher atom number in this case might lead to systematic deviations in the temperature measurement near degeneracy due to collisional hydrodynamic expansion. However, further investigation of the thermometry is beyond the scope of this work.

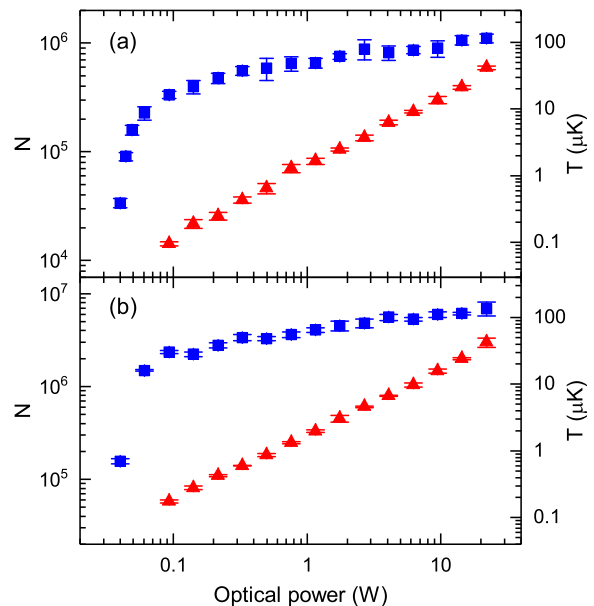


FIG. 6. (Color online) Total number of atoms N (blue squares) and temperature T (red filled circles) at various points during forced evaporative cooling performed at 940 G. The x-axis displays the optical power per beam of the ODT at which the evaporation ramp was halted. Panel (a) the ODT was loaded from the gray molasses, time constant: 10 s (b) the ODT was loaded from the UV MOT, time constant: 3 s.

V. CONCLUSION

In summary, we have demonstrated a simple experimental implementation of a gray molasses and utilized it to produce a quantum degenerate gas of lithium. This was achieved by rapid switching of the injection seeding of a diode laser between the D_2 and D_1 light needed for loading into a standard MOT and gray molasses cooling, respectively. We demonstrated how a beat between seeding and output light of the diode laser can be used as a convenient method to monitor the correct operation of the gray molasses experiment. The gray molasses was characterized and compared with the UV MOT where narrow-line cooling is applied. While both methods reach similar sub-Doppler temperatures, the low-intensity gray molasses yields a larger cloud containing a higher number of atoms, whereas the UV MOT produces a smaller but denser cloud with a higher phase-space density. This resulted in a higher transfer efficiency of the atoms into a crossed optical dipole trap from the UV MOT than from the GM. After evaporative cooling this translated into a proportionally larger sample size at quantum degeneracy. We therefore find that with minimal experimental effort, the gray molasses allows us to obtain a quantum degenerate cloud with on the order of a few 10^5 atoms. For many purposes, such as the modern experiments on quantum gas microscopy, this atom number is already sufficient. Where a larger degenerate cloud is needed, and certain additional experimental effort is acceptable,

the UV MOT offers a significant improvement of the sample size.

Acknowledgments

This research is supported by the National Research Foundation, Prime Ministers Office, Singapore and the Ministry of Education, Singapore under the Research Centres of Excellence program.

-
- [1] J. Sebastian, Ch. Gross, K. Li, H. C. J. Gan, W. Li, and K. Dieckmann, *Phys. Rev. A* **90**, 033417 (2014).
- [2] I. Bloch, J. Dalibard, and W. Zwerger, *Rev. Mod. Phys.* **80**, 885 (2008).
- [3] C. Gross and I. Bloch, *Science* **357**, 995 (2017).
- [4] C. Fort, A. Bambini, L. Cacciapuoti, F. Cataliotti, M. Prevedelli, G. Tino, and M. Inguscio, *The European Physical Journal D - Atomic, Molecular, Optical and Plasma Physics* **3**, 113 (1998).
- [5] P. M. Duarte, R. A. Hart, J. M. Hitchcock, T. A. Corcovilos, T.-L. Yang, A. Reed, and R. G. Hulet, *Phys. Rev. A* **84**, 061406 (2011).
- [6] D. C. McKay, D. Jervis, D. J. Fine, J. W. Simpson-Porco, G. J. A. Edge, and J. H. Thywissen, *Phys. Rev. A* **84**, 063420 (2011).
- [7] Ch. Gross, H. C. J Gan, and K. Dieckmann, *Phys. Rev. A* **93** 053424 (2016).
- [8] D. Boiron, C. Triché, D. R. Meacher, P. Verkerk, and G. Grynberg, *Phys. Rev. A* **52** R3425(R) (1995).
- [9] D. Boiron, A. Michaud, P. Lemonde, Y. Castin, C. Salomon, S. Weyers, K. Szymaniec, L. Cognet, and A. Clairon, *Phys. Rev. A* **53** R3734(R) (1996).
- [10] D. R. Fernandes, F. Sievers, N. Kretzschmar, S. Wu, C. Salomon, and F. Chevy, *Europhys. Lett.* **100**, 63001 (2012).
- [11] A. T. Grier, I. Ferrier-Barbut, B. S. Rem, M. Delehaye, L. Khaykovich, F. Chevy, and Christophe Salomon, *Phys. Rev. A*, **87**, 063411 (2013).
- [12] D. Nath, R. K. Easwaran, G. Rajalakshmi, and C. S. Unnikrishnan, *Phys. Rev. A* **88**, 053407 (2013).
- [13] G. Salomon, L. Fouché, P. Wang, A. Aspect, P. Bouyer, and T. Bourdel, *Europhys. Lett.* **104**, 63002 (2013)
- [14] A. Burchianti, G. Valtolina, J. A. Seman, E. Pace, M. De Pas, M. Inguscio, M. Zaccanti, and G. Roati, *Phys. Rev. A* **90**, 043408 (2014).
- [15] F. Sievers, N. Kretzschmar, D. R. Fernandes, D. Suchet, M. Rabinovic, S. Wu, C. V. Parker, L. Khaykovich, C. Salomon, and F. Chevy, *Phys. Rev. A* **91**, 023426 (2015).
- [16] G. Colzi, G. Durastante, E. Fava, S. Serafini, G. Lamporesi, and G. Ferrari, *Phys. Rev. A* **93**, 023421 (2016).
- [17] H. Z. Chen, X. C. Yao, Y. P. Wu, X. P. Liu, X. Q. Wang, Y. X. Wang, Y. A. Chen, and J. W. Pan, *Phys. Rev. A* **94**, 033408 (2016).
- [18] G. D. Bruce, E. Haller, B. Peaudecerf, D. A. Cotta, M. Andia, S. Wu, M. Y. H. Johnson, B. W. Lovett, and S. Kuhr, *Journal of Physics B: Atomic, Molecular and Optical Physics* **50**, 095002 (2017).
- [19] S. Rosi, A. Burchianti, S. Conclave, D. S. Naik, G. Roati, C. Fort, and F. Minardi, *Scientific Reports* **8**, 1301 (2018).
- [20] M. S. Shahriar, P. R. Hemmer, M. G. Prentiss, P. Marte, J. Mervis, D. P. Katz, N. P. Bigelow, and T. Cai, *Phys. Rev. A* **48**, R4035 (1993).
- [21] G. Grynberg and J.-Y. Courtois, *Europhys. Lett.* **27**, 41 (1994).
- [22] M. Weidemüller, T. Esslinger, M. A. Ol'shanii, A. Hemmerich, and T. W. Hänsch, *Europhys. Lett.* **27**, 109 (1994).
- [23] M. Landini, S. Roy, L. Carcagní, D. Trypogeorgos, M. Fattori, M. Inguscio, and G. Modugno, *Phys. Rev. A* **84**, 043432 (2011).
- [24] M. S. Safronova, U. I. Safronova, and C. W. Clark, *Phys. Rev. A* **86**, 042505 (2012).
- [25] G. Zürn, T. Lompe, A. N. Wenz, S. Jochim, P. S. Julienne, and J. M. Hutson, *Phys. Rev. Lett.* **110**, 135301 (2013).
- [26] L. Luo, B. Clancy, J. Joseph, J. Kinast, A. Turlapov, and J. E. Thomas, *New J. Phys.* **8**, 213 (2006).